Processing and Application of Ceramics 13 [3] (2019) 219–228
https://doi.org/10.2298/PAC1903219F

Evidence of ferroelectric behaviour in $CaCu_3Ti_4O_{12}$ thin films deposited by RF-sputtering

Cesar R. Foschini[1], Bruno Hangai[2], Pedro Paulo Ortega[2,*], Elson Longo[3], Mário Cilense[3], Alexandre Z. Simões[2,*]

[1]*São Paulo State University (UNESP) – School of Engineering of Bauru, Av. Eng. Luiz Edmundo C. Coube 14-01, CEP 17033-360, Bauru, São Paulo, Brazil*
[2]*São Paulo State University (UNESP) – School of Engineering of Guaratinguetá, Av. Dr. Ariberto Pereira da Cunha 333, CEP 12.516-410, Guaratinguetá, São Paulo, Brazil*
[3]*São Paulo State University (UNESP) – Chemistry Institute, R. Prof. Francisco Degni 55, CEP 14800-900, Araraquara, São Paulo, Brazil*

Received 3 October 2018; Received in revised form 15 May 2019; Received in revised form 15 June 2019; Accepted 5 July 2019

Abstract

The origin of abnormal ferroelectric and unusual piezoelectricity in the polycrystalline $CaCu_3Ti_4O_{12}$ (CCTO) thin films deposited by RF-sputtering on Pt/Ti/SiO_2/Si (100) substrates was explored. The CCTO thin films, deposited at room temperature followed by annealing at 600 °C for 2 h in a conventional furnace, have a cubic structure with lattice parameter a = 7.379 ± 0.001 Å and without any secondary phases. No polarization loss up to 10^{10} switching cycles, with a switched polarization ΔP of 30 μC/cm² measured at 400 kV/cm was evidenced. The piezoelectric coefficient investigated by piezoresponse force microscopy (PFM) was approximately 9.0 pm/V. This may be the very first example of exploring the origin of ferroelectric behaviour for a material that possesses space charge polarization with highly resistive grain boundaries in the polycrystalline state.

Keywords: *calcium copper titanate, CCTO, ferroelectricity, RF-sputtering, thin films*

I. Introduction

Calcium copper titanate ($CaCu_3Ti_4O_{12}$), commonly referred to as CCTO, has gained much interest for being a potential candidate for microelectronic applications, such as capacitors, microwave devices, gas and humidity sensors, switching, energy storage devices, power systems and memory devices [1–3], mainly due to its extremely high dielectric permittivity (ε_r). Firstly discovered by Subramanian *et al.* [4], the colossal dielectric constant of CCTO is of the order of 10^5 at room temperature, which is frequency independent in the 10^2–10^6 Hz range and temperature insensitive from 100 to 600 K [2,5,6].

Over the last two decades, great effort has been put into unravelling the origins of the colossal dielectric constant of CCTO in the form of bulk and crystalline thin films [6–13]. Previously intrinsic mechanisms related to the crystal structure have been studied as a potential cause of CCTO giant permittivity. However, it is now clear that such high dielectric constant is extrinsic in nature and rather common in multiple CCTO based compounds [14]. In polycrystalline CCTO this extrinsic cause can be explained by the Internal Barrier Layer Capacitor (IBLC) model, which is based on n-type semiconducting grains separated by insulating grain boundaries [2,8]. Accordingly, the interfacial polarization mechanism by larger dipoles induced across grain boundaries is understood as the main contributor. This is very rare since many other perovskite ferroelectrics do not possess the intrinsic nature of interfacial polarization. For instance, in $BaTiO_3$ a giant dielectric constant is induced by interfacial polarization after post

*Corresponding author: tel: +98 71 3613 3399,
e-mail: *pedro.ortega@hotmail.com.br* (P.P. Ortega),
alezipo@yahoo.com (A.Z. Simões)

heat treatment in a reducing atmosphere to control the chemical states of the grain boundaries [15–17].

These outstanding electrical properties are quite unusual, since CCTO exhibits a body-centred cubic perovskite structure (AB_3O_4), where A sites are occupied by Cu^{2+} and Ca^{2+} cations and B sites are occupied by Ti^{4+} cations with tilted [TiO_6] octahedra facing each other [6,14,18], i.e. the compound is not usually ferroelectric. Despite numerous studies, including quantum chemical calculations [19], the origin of this high dielectric constant remains unclear. Impedance spectroscopy has proven that such ceramics consist of semiconducting grains and insulating grain boundaries [2]. The results from Sinclair *et al.* [20] suggest that the high dielectric constant is actually an internal grain boundary barrier layer capacitance, i.e. it is a grain boundary effect that is not linked to the perovskite crystal structure. To justify the dramatic decrease in permittivity below 100 K, it has been suggested that the dipoles "freeze" (relax out) at low temperatures, besides their excellent piezoelectric and dielectric properties.

Several physical and chemical techniques have been used to deposit high-quality CCTO films, such as metal organic chemical vapour deposition (MOCVD), sol-gel method, chemical solution deposition, pulsed laser deposition (PLD) and radio frequency (RF) sputtering [3,6,9,12]. Among these techniques, RF-sputtering is the most accessible method due to several advantages: relatively cost-effective, low process temperature, easy-to-control parameters, high deposition rate, uniform microstructure, scalability to large areas, homogeneity over large areas, reproducibility and very good stability [21,22]. Moreover, RF-sputtering has also proven to be a promising approach for producing thin-film capacitors in integrated circuits.

In our previous work, CCTO thin films were obtained by RF-sputtering from the CCTO target with relatively high values of the profile *R*-factors which reflects the good statistics of the data; consistently, the Le Bail fit with identical values of profile coefficients yielded a space group $Im3$, $a = 7.39612(3)$ Å, $Z = 2$, $\chi^2 = 2.64$, $R_p = 12.0\%$, $R_{wp} = 16.5\%$, $R_B = 4.35\%$, $R_F = 3.84\%$ [23]. Refinement was limited to isotropic ADPs – anisotropic refinement did not yield any significant improvement in the fit quality and components of ADP tensors were refined with large uncertainties. The absence of by-products such as $CaTiO_3$ and TiO_2 indicates that the CCTO film crystallized in the pseudocubic phase with no changes during the refinement. From the low S values ($S = R_{wp}/R_{exp} = 1.4\%$) it can be assumed that the refinement of the CCTO phase was successfully performed with all the investigated parameters close to literature data [24,25].

Wu *et al.* [26] have deposited polycrystalline CCTO thin films with different thicknesses on Pt/Ti/SiO_2/Si substrates and found that their dielectric properties are comparable to those observed in the CCTO films grown on oxide substrates. It is well known that the bottom electrode plays an important role during the fabrication of dielectric or ferroelectric thin films. The electrode materials are required to have certain properties, such as high metallic conductivity, sufficient resistance against oxidation and a good film adhesion. Therefore, platinum, one of the few metals that satisfy these requirements, has been used as a bottom electrode in high dielectric constant thin film capacitors [27]. High dielectric constant ε_r thin films have been studied in order to pursue better device performances in various passive and active components. These devices require high capacitance to store more charges and/or to reduce the operating voltage [10,12,28–31]. Since the dielectric behaviour for generating high permittivity is generally based on ionic and dipolar (orientational) polarization mechanisms, ferroelectric perovskite materials showing spontaneous polarization at room temperature, including representative $BaTiO_3$ and Pb(Zr,Ti)O_3, are preferably adjusted for the highest ε_r thin film applications [32–34].

This work investigates CCTO thin films processed at room temperature by sputtering with an anomalous remnant polarization (P_r) of 8.3 μC/cm^2, which is more promising as compared to other reported values for thin film materials. The origin of such abnormal behaviour, in conjunction with the polarization mechanism, is explored here with supporting evidence for the chemical states and ferroelectric domain formation. Therefore, the main goal is to discuss the ferro/piezo response of highly dense $CaCu_3Ti_4O_{12}$ polycrystalline film deposited on Pt/Ti/SiO_2/Si substrates by RF-sputtering. It is useful to understand the nature of interfacial polarization mechanism by larger dipoles induced across grain boundaries as the main contributor for ferro/piezo response of CCTO thin films, which could be widely applied in active electronic devices that require high dielectric constant and near room temperature processing.

II. Experimental procedure

The CCTO targets were prepared by conventional solid-state reaction. Calcium carbonate, copper oxide and titanium dioxide (>99% purity and <1 μm) were mixed by ball milling in ethanol for 12 h. After drying, the powder was calcined at 900 °C for 12 h. The calcined powder was mixed with a binder (PVA) and uniaxially pressed into discs of approximately 50 mm in diameter and 3 mm thickness and sintered at 1100 °C for 3 h. From these targets, nanostructured $CaCu_3Ti_4O_{12}$ films deposited on Pt/Ti/SiO_2/Si substrates were obtained by RF-sputtering at 300 °C as previously published elsewhere [23]. Deposition of CCTO films were carried out by sputtering a CCTO target in pure argon and oxygen at 2×10^{-2} mbar and 150 W RF power. The distance between target and substrate was kept constant at 15 cm and the depositions lasted 2 h at room temperature (Fig. 1).

The thickness of the annealed films was analysed

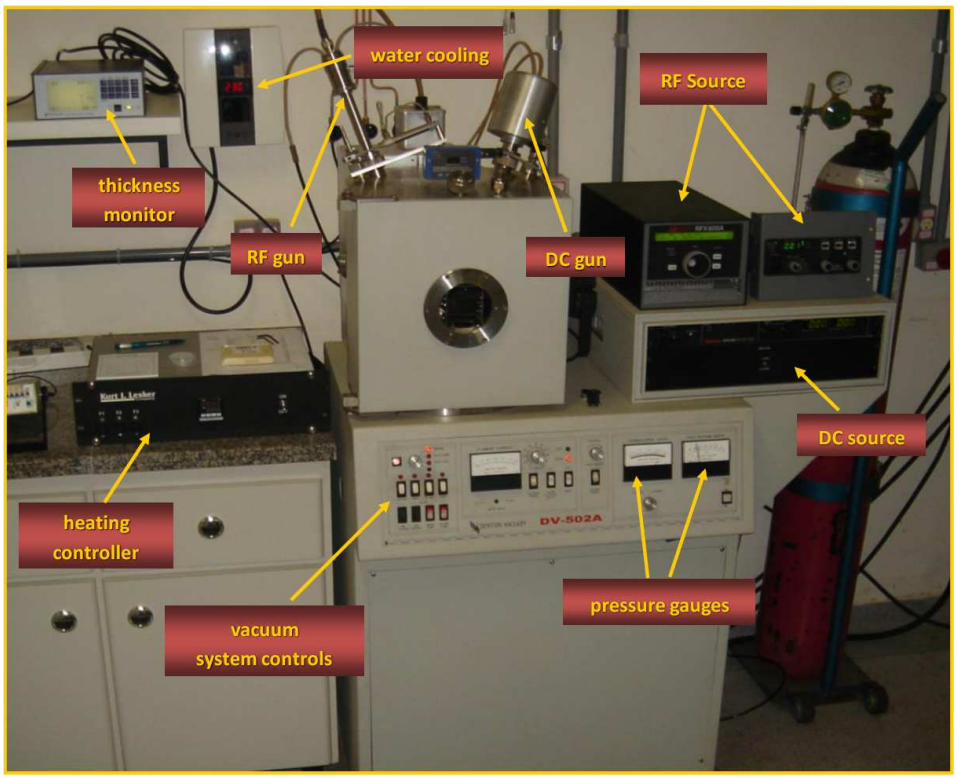

Figure 1. Schematic illustration of RF-sputtering system used to produce CCTO thin films in a conventional furnace

using a field emission gun scanning electron microscope (FEG-SEM, JEOL, Model 7500F). For electrical DC and AC measurements, top Au electrodes (diameter: 200 μm) were deposited by sputtering through a shadow mask at room temperature acquiring a metal-semiconductor-metal (MSM) capacitor configuration. The XPS analysis was carried out at a pressure of less than 10^{-7} Pa using a commercial spectrometer (UNI-SPECS UHV) to verify the changes in surface chemical composition of the treated specimens. The Mg K line was used (h = 1253.6 eV) and the analyser pass energy was set to 10 eV. The inelastic background of the Cu 2p, Ca 2p, Ti 2p and O 1s electron core-level spectra were subtracted using Shirley's method. The composition of the near surface region was determined with an accuracy of ±10% from the ratio of the relative peak areas corrected by Scofield's sensitivity factors of the corresponding elements. The spectra were fitted without placing constraints using multiple Voigt profiles. The width at half maximum (FWHM) varied between 1.2 and 2.1 eV and the accuracy of the peak position was ±0.1 eV. The XPS spectroscopy provided information on the bonding structure and composition of the near surface region of the material. The results of the quantitative analysis obtained for the as-grown reference and samples prepared in oxygen and nitrogen atmosphere are listed in Table 1. The hysteresis loop measurements were carried out on the films with a Radiant Technology RT6000HVS at a measured frequency of 60 Hz. These loops were traced using the Charge 5.0 program included in the software of the RT6000HVS in a virtual ground mode test device. The fatigue and retention characteristics of the ferroelectric capacitors were carried out at room temperature by using a Radiant Technology RT6000HVS test system at a constant applied electric field of 150 kV/cm. PUND measurements ($\Delta P = P^* - P^\wedge$) were also performed, where P^* is the switched polarization between two opposite polarity pulses and $P^\wedge$ is the non-switched polarization between the same two polarity pulses. $P^* - P^\wedge$ or $-P^* - (-P^\wedge)$ denote the switchable polarization, which is an important variable for nonvolatile memory application. Measurements of the real (C') and the imaginary (C'') part of the complex capacitance were performed with a frequency response analyser (HP 4192) using frequencies ranging from 100 Hz up to 1 MHz, with an amplitude voltage of 1 V. Complex impedance plots were measured at voltages ranging from 1 to 5 V. Piezoelectric measurements were carried out using a setup based on an atomic force microscope in a multimode scanning probe microscope with Nanoscope IV controller (Veeco FPP-100). In our experiments, piezoresponse images of the films were ac-

Table 1. Atomic concentrations of CCTO RF samples treated in oxygen atmosphere

Element	Concentration [at.%]*	
	CCTO RF	CCTO RF-O_2
Ca	5.3	4.9
Cu	14.1	20.4
Ti	14.3	12.3
O	66.2	61.1
S	-**	1.3

* Estimated error: ±10%
** Below the detection limit

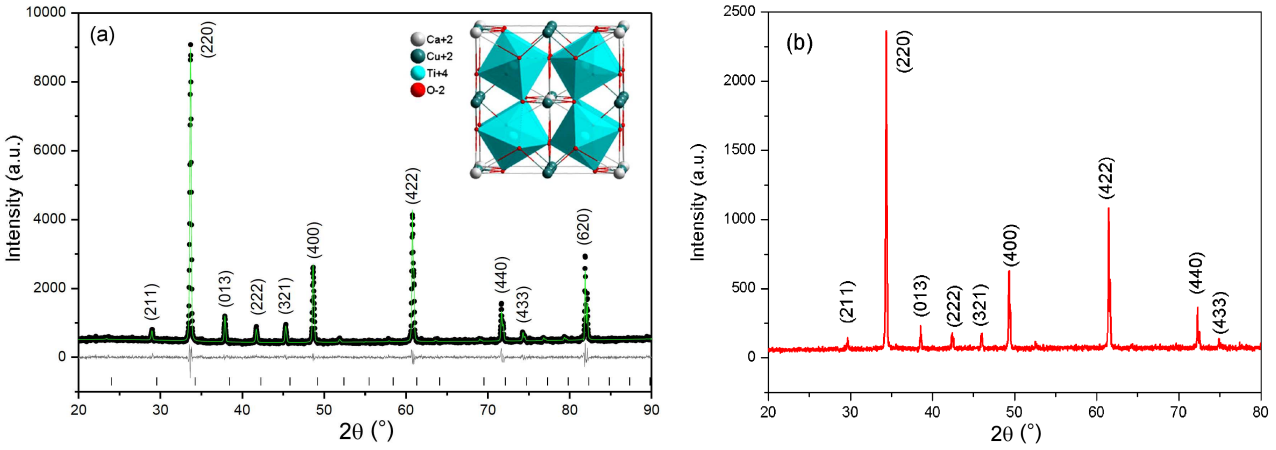

Figure 2. X-ray diffraction data for the CCTO target prepared by conventional solid-state reaction (a) and the CCTO thin film deposited by RF-sputtering at 300 °C and annealed at 600 °C for 2 h in a conventional furnace (b)

quired in ambient air by applying a small AC voltage with amplitude of 2.5 V (peak to peak) and a frequency of 10 kHz while scanning the film surface. To apply the external voltage, we used a standard gold coated Si_3N_4 cantilever with a spring constant of 0.09 N/m. The probing tip, with an apex radius of about 20 nm, was in mechanical contact with the uncoated film surface during the measurements. Cantilever vibration was detected using a conventional lock-in technique. The out-of-plane (*OP*) and in-plane (*IP*) piezoresponse images of the as-grown films after applying a bias of −12 V, on an area of 2 μm × 2 μm, and then an opposite bias of +12 V in the central 1 μm × 1 μm area were employed. For comparison, the topography of the film was also analysed. To obtain the domain images of the films, a high voltage that exceeds the coercive field was applied during scanning.

III. Results and discussion

Figure 2a shows the X-ray diffraction patterns of the CCTO target. Besides the perovskite phase, no other phase was observed. Our XRD data confirm the presence of a cubic crystal system [5,35–37]. The inset in Fig. 2a illustrates the CCTO crystal structure, with Ti atoms inside the octahedra, O atoms at the corners of the octahedra, Ca atoms at the corners of the network and Cu atoms at the half of the inner edges. No evidence of secondary phases, crystallographic symmetry lowering, reflection splitting or superlattice reflections were found. According to the XRD pattern, all diffraction peaks can be indexed to $CaCu_3Ti_4O_{12}$ (JCPDS 075-2188) with a cubic structure and lattice parameter (*a*) of 7.379 ± 0.001 Å. This is slightly shorter than the lattice parameter of CCTO previously reported [38]. XRD pattern of the thin film deposited on $Pt/Ti/SiO_2/Si$ substrate by RF-sputtering and annealed at 600 °C for 2 h is shown in Fig. 2b. According to the XRD pattern, all diffraction peaks can be indexed to $CaCu_3Ti_4O_{12}$. The characteristic peaks of Pt substrate cannot be observed in the pattern due to the low grazing angle employed to determine the XRD data. The thin film is polycrystalline in nature and free from secondary phases. Differences between the CCTO target and the thin film deposited on $Pt/Ti/SiO_2/Si$ patterns can be attributed to the characteristics of the Pt electrode which decreases the interfacial reactions between the main phase and the bottom electrode. We assume that Pt electrode play an important role of nucleation site for the formation of CCTO thin films. The positive role may be caused by the decrease in the nucleation activation energy that allows us to obtain a good crystallization at this temperature.

FEG-SEM image along with the cross-section view as an inset was used to investigate the structural morphology of the CCTO film (Fig. 3a). The film deposited by RF-sputtering shows good adhesion to the $Pt/Ti/SiO_2/Si$ (100) substrate and consists of homogeneous and crack-free microstructure formed from interconnected nanoparticles, with an average thickness of 600 nm. The grains present rounded morphology and are uniformly distributed, with an average mean grain size close to 13 nm. Most of the pores are nanostructured, with sizes around 5 nm. It is noted that the CCTO film consists of several grain layers. In the first layer the grains align neatly, suggesting the solid-phase mechanism for the film growth. Though the other layers show random-like assembly of grains, the resultant surface is rather flat. It is noteworthy to say that the homogeneous microstructure of CCTO film may reduce leakage current, enabling charge carriers to flow uniformly onto it [39]. Energy dispersive spectroscopy (EDS) stage (Fig. 3b) attached to the field emission scanning electron microscopy revealed no secondary phases. The mapping of the oxygen element shows that the grain boundary region has the same composition as the grain. The absence of precipitates at the grain boundaries is certainly important in defining the ferro/piezo behaviour of such films once the polar properties are stabilized by charged domain walls which interact with oxygen vacancies and inhibit the unusual piezoelectricity in crystalline state. During the application of the applied electric field, an accumulation of oxygen vacancies near the electrode-

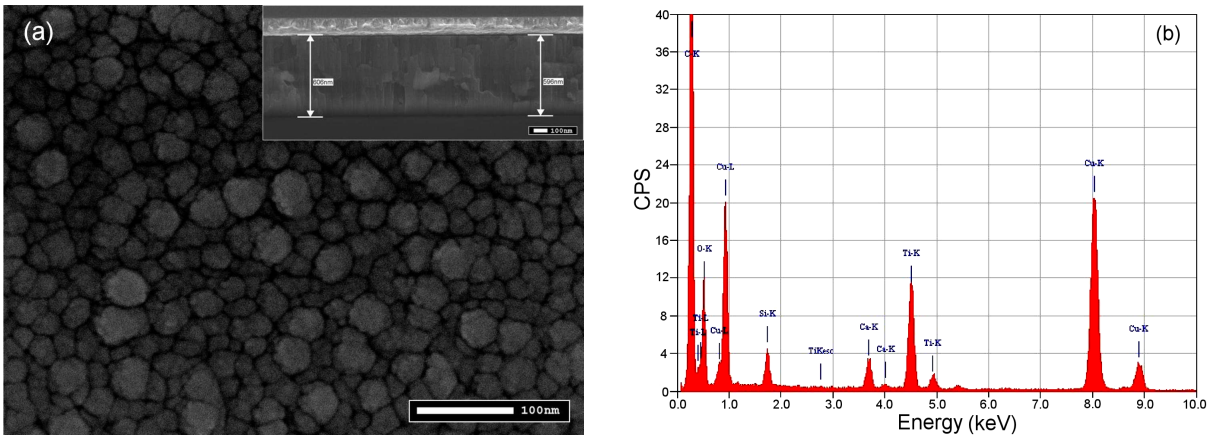

Figure 3. FEG-SEM for CCTO thin film deposited by RF-sputtering at 300 °C and annealed at 600 °C for 2 h in a conventional furnace and (b) EDS analysis of a sintered CCTO film

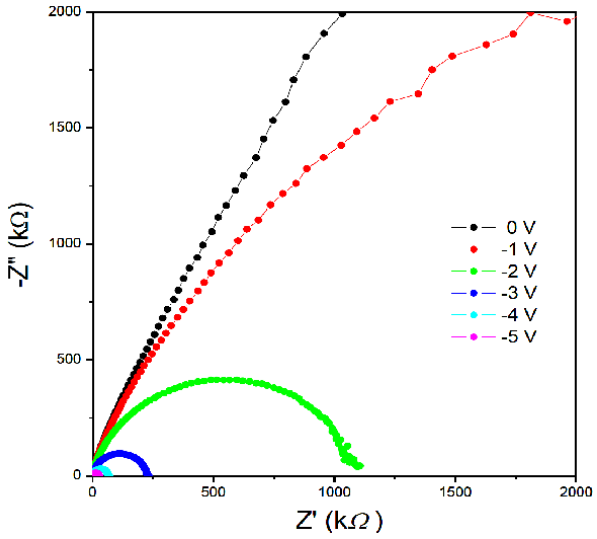

Figure 4. Complex impedance plot for CCTO thin film deposited by the RF-sputtering at 300 °C and annealed at 600 °C for 2 h in a conventional furnace

film interface might occur, which reduces the abnormal ferroelectric behaviour.

Figure 4 shows the complex impedance plots for the capacitor which can be modelled and analysed using two parallel RC elements, each corresponding to one of the observed semicircles, in series with a connection resistance. A single large semicircle is displayed for voltages up to 1.0 V, while for voltages higher than 2.0 V, a shoulder develops in the higher frequency range. The appearance of the second semicircle with a Z_0 value of about 10 Ω can be ascribed to the resistance from cables and probe tips. Our results suggest that the dielectric response is provided by the electrode/CCTO interfaces and not from the CCTO grains. Interfaces' resistance R_{int} and capacitance C_{int} measured at room temperature were extracted using the relation $\omega \cdot R \cdot C = 1$ and the obtained values are $R_{int} \cdot S = 0.1\,\mathrm{M\Omega\,mm^2}$ and $C_{int}/S = 30\,\mathrm{nF/mm^2}$.

To explore the origin of the abnormal ferroelectric behaviour, we measured the polarization electric field (*P-E*) hysteresis loop curves of the crystalline CCTO thin films deposited by RF-sputtering (Fig. 5a). The CCTO thin films exhibited typical characteristics of ferroelectric materials, which suggests that by increasing the applied electric field, the remnant polarization and coercive field also increased, implying that these films possess a ferroelectric nature. Crystalline films contain fewer oxygen vacancies at the surface considering the semiconductor area with high surface to volume ratio. Therefore, the existence of two different Ti clusters, basically $[TiO_6]$ and $[TiO_5 \cdot V_O^{\bullet}]$ reduces the conductivity of the film as the oxygen vacancies would induce new energy levels in the band gap. Considering that such oxygen vacancies are positively charged, most of the electrons around oxygen vacancies are released and then the charge transfer occurring from $[TiO_6]$ and $[TiO_5 \cdot V_O^{\bullet}]$ clusters creates electron and hole polarons that can be designated as Jahn-Teller bipolarons. The charge trapping favours the appearance of dielectric behaviour [19]. At room temperature, the film shows a typical ferroelectric loop, and the values of nearly saturation polarization (P_s), remnant polarization (P_r) and the electric coercivity (E_c) are 40.0 μC/cm^2, 8.3 μC/cm^2 and 40.0 kV/cm, respectively. The observed loop clearly indicates the ferroelectric ordering of the dipole moment configuration due to the spontaneous polarization of the sample. Thus, it is established that the present sample is in a state where electric ordering is present. The PUND measurement (Fig. 5b) allows to obtain the real switched polarization properties. The switched polarization (ΔP) obtained at 400 kV/cm is 30 μC/cm^2 and began to saturate at 700 kV/cm, being consistent with the $2P_r$ values from the *P-E* hysteresis loop. Moreover, in the range of 1 μs to 1 ms the polarization showed weak pulse width dependence, as shown in Fig. 5c. This response reveals that the measured polarization switching is an intrinsic property of CCTO thin films, and is not dominated by leakage, which was a critical obstacle in determining the ferroelectric property of dielectric materials.

The fatigue characteristics of the CCTO capacitor are displayed in Fig. 6a. As it can be seen, there is no polarization loss up to 10^{10} switching cycles. Degradation

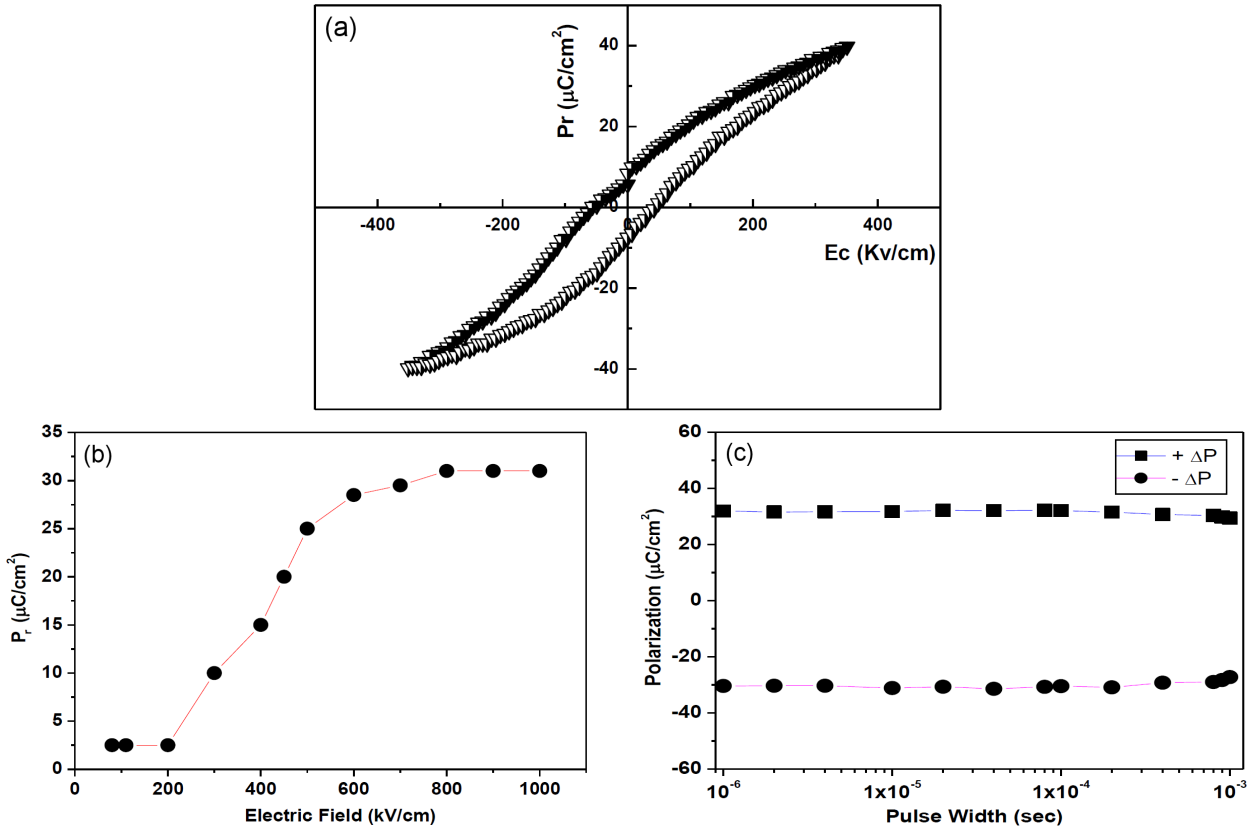

Figure 5. *P-E* loop (a), pulsed polarization (Δ*P*) as a function of an applied voltage (b) and pulse width dependence of switched polarization (Δ*P*) in the range from 1 μs to 1 ms (c) for CCTO thin film deposited by RF-sputtering at 300 °C and annealed at 600 °C for 2 h in a conventional furnace

of the CCTO thin film is not observed while using the Pt interface electrode as buffer layer. Usually, the loss of switching polarization with repeated polarization reversal is due to pinning of the domain wall, which inhibits switching of the domain affected by induced internal space charge at domain boundaries. Typical mechanisms for domain wall pinning include pinning due to the electron charges trapped by oxygen vacancies. Considering that the CCTO film is fatigue-free, we assume that the accumulation of oxygen vacancies near the interface is reduced and consequently this implies less charge trapping and domain wall pinning in the interface region. Therefore, the effects of Pt as a substrate on the fatigue behaviour of the CCTO films may be attributed to its function as an oxygen vacancy sink. Polarization loss, characteristic of retention behaviour, is the time-dependent change of the polarization state in the ferroelectric film. After a long time, it can be caused in the ferroelectric memory device (Fig. 6b). After a retention time of 10 s, the initial polarization decayed to a nearly steady-state value, while after 10^4 s, the polarization loss was about 20% of the value measured at $t = 1$ s. These results point out that the presence of an internal electric field due to the bias effect arising from the incomplete screening of the depolarization field can lead to retention loss in the ferroelectric CCTO thin film. The leakage current was not eliminated if the bias was retained during this retention period due to the space charge present in the film. We can consider that the polarization charges are not completely compensated by the electrode charges, because polarization and electrode charges are separated from each other. The existence of a spatial variation of polarization near the electrode is the origin of charge separation and also the possible existence of a low dielectric constant surface layers as well as the finite thickness of the compensation charge layers in the electrodes.

In order to further ensure the intrinsic nature of the observed ferroelectric behaviour for the CCTO thin films, piezoresponse force microscopy (PFM) studies were performed, as shown in Fig. 7a-c. The images show that each region gives a uniform piezoelectric response, implying a homogeneous polarization state, with the misalignment of the squares being due to drift in the AFM scanner. The corresponding topography reveals a flat surface, with a roughness comparable to the rest of the film (Fig. 7a). The PFM image of the thin film deposited by RF-sputtering clearly shows a bright and dark contrast-mixed state, which was extracted by different piezoresponse amplitudes, indicating the presence of electric domains with ~20 nm scale. The direction of the polarization is associated with contrast in these images. The perpendicular component of the polarization can be switched between two stable states in the PFM images: bright and dark contrast inside and outside of the square area. Regions without piezore-

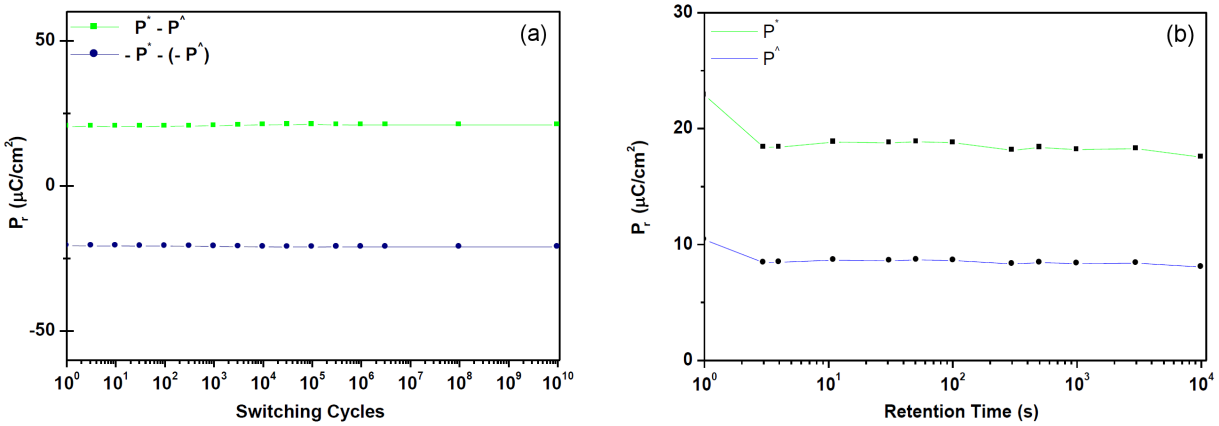

Figure 6. Fatigue as a function of polarization cycles (a) and P^* and $P\hat{}$(b) for CCTO thin film deposited by RF-sputtering at 300 °C and annealed at 600 °C for 2 h in a conventional furnace for a retention time up to 1×10^4 s and applied electric field of 150 kV/cm

sponse exhibit a strong contrast in the PFM images. The polarization vector oriented toward the bottom electrode hereafter referred to as down polarization (Fig. 7b) is visualized by white regions in the out-of-plane PFM images while the dark regions correspond to domains oriented upward, referred to as up polarization. Grains which exhibit no contrast change are associated with zero out-of-plane polarization. Some of the grains exhibit a white contrast associated to a component of the polarization pointing toward the bottom electrode. On the other hand, in the in-plane PFM images (Fig. 7c) the contrast changes were associated with changes of the in-plane polarization components. In this case, the white contrast indicates polarization, e.g. in the positive direction of the *y*-axis, while dark contrast is given by in-plane polarization components pointing to the negative part of the *y*-axis. It is very interesting to observe the formation of domains from the hysteresis loops and direct amplitude images. The formation of domains observed from the hysteresis loops and direct amplitude

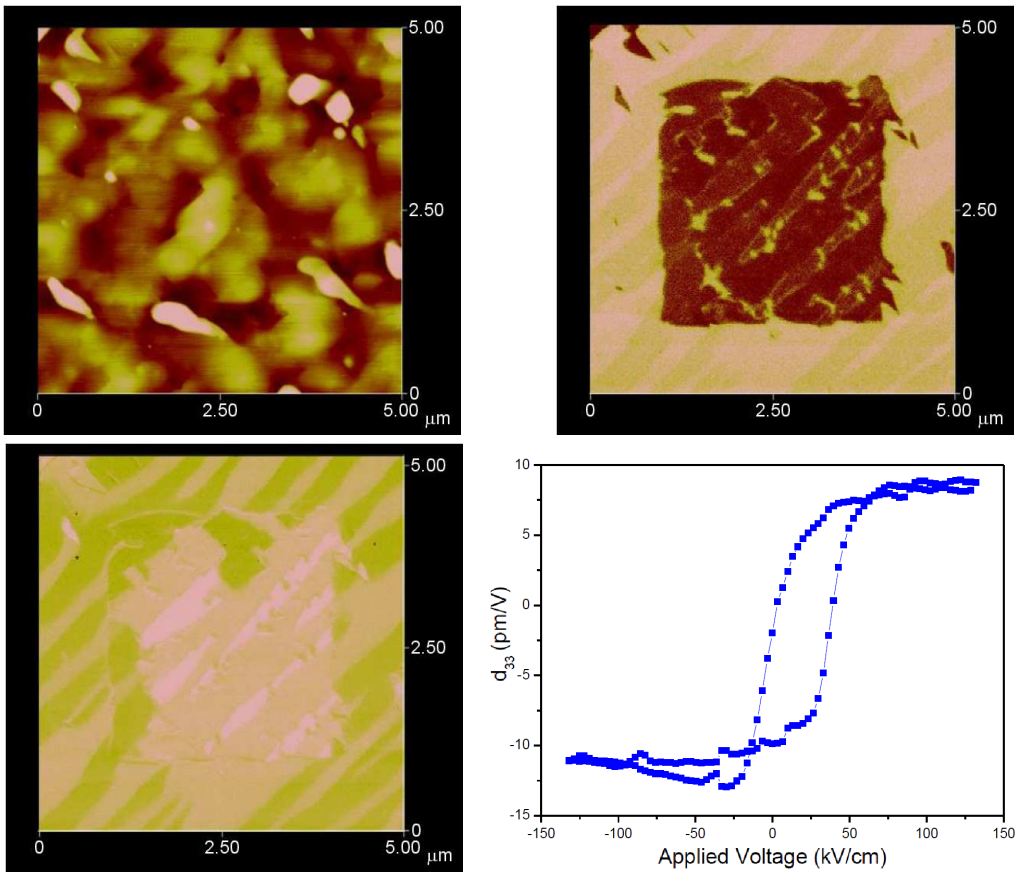

Figure 7. Topography (a), out-of-plane (b), in-plane (c) and piezoresponse loop - d_{33} versus applied electric field (d) for CCTO thin film deposited by RF-sputtering at 300 °C and annealed at 600 °C for 2 h in a conventional furnace

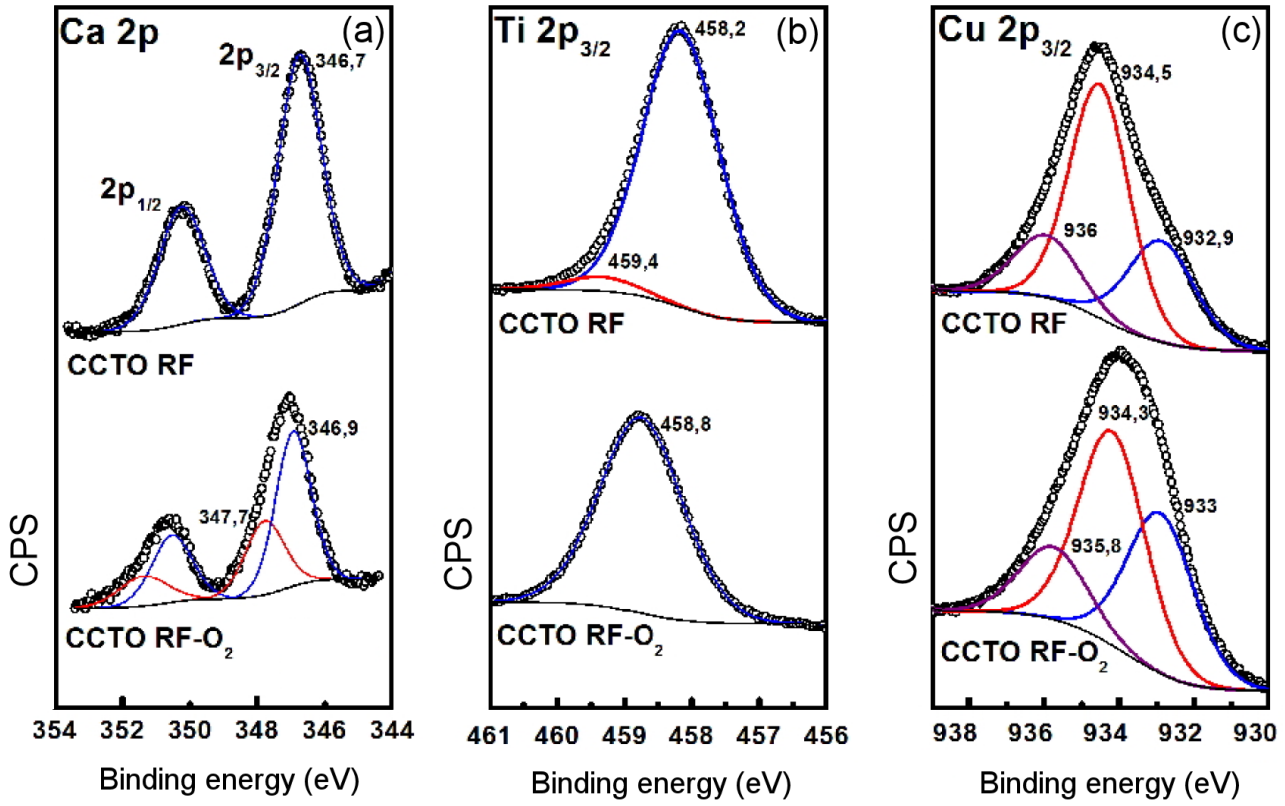

Figure 8. XPS spectra for CCTO thin film deposited by the RF-sputtering at room temperature and annealed at 600 °C for 2 h in a conventional furnace showing: (a) Spin orbit doublets of Ca 2 $p_{3/2}$ and Ca 2 $p_{1/2}$, (b) Ti 2 $p_{3/2}$ and (c) Cu 2 $p_{3/2}$

image may be due to a higher Ti^{4+} concentration, as observed by XPS technique. Figure 7d shows the piezoelectric hysteresis loop obtained for the CCTO film. The piezoresponse signal is directly associated with the polarization switching and ferroelectric properties of the sample. It depends on the grain orientation and surface characteristics as the films are polycrystalline in nature. A d_{33} value of ~9.0 pm/V revealed that the CCTO film behaves as a piezoelectric material showing that it is easy to switch the domains. Since our measurements were performed on a local area that has a relatively intricate field distribution and vibrational modes, it is difficult to compare these values to the piezoelectric coefficients of bulk materials. Taking into account the differences in the piezoelectric loop with the hysteresis data, we consider only the contribution of the piezoelectric domains. Therefore, as expected, the piezoelectric response signal is a consequence of strain energy and pining effect of charged defects due to the charge transference of the oxygen.

As shown in Figure 8 and Table 1, the existence of two different Ti clusters, basically TiO_6 and $[TiO_5 \cdot V_O^{\bullet}]$ can be explained considering the existence of species sub-coordinated with titanium. In other words, disordered clusters associated to oxygen vacancies as $[TiO_5 \cdot V_O^{\bullet}]$. The oxygen vacancies would be easily accommodated in the TiO_5 local substructure. Thus, the increase of Cu–O bonding causes structural disorder in the TiO_6 octahedron network. The charge transfer between $[TiO_5 \cdot V_O^{\bullet}]$ clusters and Cu'_{Cu} defects creates positive and negative polarons and the combination of both constitutes a new entity called Jahn-Teller bipolaron, which causes additional strain. Except the lower Ti content, the composition of the reference sample is close to the nominal stoichiometry of $CaCu_3Ti_4O_{12}$. The O_2 treatment led to an excess of Cu, due to Cu segregation on the surface, forming copper oxide crystals. To get a better insight on the processes occurring on the surface, the evolution of the structural components was analysed by the deconvolution of the Cu 2 $p_{3/2}$,Ti 2 $p_{3/2}$ and Ca 2 p spectra. The high-resolution Cu 2 $p_{3/2}$ spectra, displayed in Fig. 8c, show three distinct surface species, which were attributed to $CuCO_3$ (935.9 eV), CuO (934.4 eV) and Cu_2O (932.8 eV) [40]. The presence of copper carbonate was evidenced by the presence of the corresponding $CuCO_3$ component in the C 1 s spectra, found at about 288.6 eV (not shown). Despite the different treatment of the samples, the only difference observed is that the intensity of the main CuO component of the CCTO RF-O_2 sample decreases slightly on the expense of the Cu_2O sub-peak. While for the reference sample the Ca 2 p spectra indicate a pure CuO phase (834.8 eV), the CCTO RF-O_2 display a second spin-orbit component, indicating the formation of a $CaSO_4$ phase [19], due to the presence of sulphur, detected on the surface (Fig. 8a). Also, the chemical bonding environment of Ti has been modified upon changed deposition conditions. The fitted Ti 2 p spec-

tra, displayed in Fig. 8b, shows a principal component at about 458.4 eV for the reference sample, related to the TiO_2 phase, and a small high energy sub-peak at 459.3 eV. The origin of the Ti 2 p sub-peak is not quite clear, but is most probably related to oxygen vacancies forming 5-fold coordinated sites in the TiO_2 lattice [41]. This is supported by the disappearance of this component for the sample prepared in the O_2 atmosphere. We could propose that the charge transfer between $[TiO_5 \cdot V_O^{\bullet}]$ clusters and Cu'_{Cu} defects facilitate domain wall movement, while ($V_O^{\bullet\bullet}$) render domain wall movement more difficult. An oxygen vacancy-acceptor ion dipole may interact upon polarization within a domain, thereby making its movement more difficult. Consequently, neutral (V_O^x) and oxygen vacancies of ($V_O^{\bullet}$) type make the movement of domain walls easier. Furthermore, low anisotropy and the formation of charge transfer between $[TiO_5 \cdot V_O^{\bullet}]$ clusters and Cu'_{Cu} defects besides the oxygen vacancies ($V_O^{\bullet}$) in the CCTO-type structure enhances the ferroelectric properties of thin films. The enhancement of Cu–O bonding causes a high degree of disorder in the network forming positions with octahedral TiO_6 structural units. Such structural units may increase the rigidity of the network and increase the values of ferroelectric parameters, as it was observed.

IV. Conclusions

Polycrystalline CCTO thin films were obtained on Pt/Ti/SiO_2/Si (100) substrates at room temperature followed by annealing at 600 °C for 2 h in a conventional furnace, with a cubic structure belonging to the $Im\bar{3}$ space group. The film deposited by the RF-sputtering technique shows good adhesion to the substrate and consists of homogeneous and crack-free microstructure formed of interconnected nanoparticles. Evidence of ferroelectricity was confirmed by a hysteresis loop and domain formation while complex impedance analysis further supported the potential dipolar polarization along with the interfacial polarization of film/electrode. The formation of domains observed from the piezoresponse can be caused by the charge transfer between $[TiO_5 \cdot V_O^{\bullet}]$ clusters and Cu'_{Cu} defects creating positive and negative polarons. The combination of both constitutes a new entity called Jahn-Teller bipolaron, which causes additional strain. In order to use this material in technical applications, a compromise between piezoelectric properties and fatigue/retention still has to be found.

Acknowledgement: The financial support of this research project by the Brazilian research funding agency FAPESP (grant number 2013/07296-2) is gratefully acknowledged.

References

1. W. Yang, S. Yu, R. Sun, R. Du, "Nano- and micro-size effect of CCTO fillers on the dielectric behavior of CCTO/PVDF composites", *Acta Mater.*, **59** (2011) 5593–5602.
2. P. Mao, J. Wang, S. Liu, L. Zhang, Y. Zhao, L. He, "Grain size effect on the dielectric and non-ohmic properties of $CaCu_3Ti_4O_{12}$ ceramics prepared by the sol-gel process", *J. Alloys Compd.*, **778** (2019) 625–632.
3. M. Ahmadipour, M.F. Ain, Z.A. Ahmad, "Effect of thickness on surface morphology, optical and humidity sensing properties of RF magnetron sputtered CCTO thin films", *Appl. Surf. Sci.*, **385** (2016) 182–190.
4. M.A. Subramanian, D. Li, N. Duan, B.A. Reisner, A.W. Sleight, "High dielectric constant in $ACu_3Ti_4O_{12}$ and $ACu_3Ti_3FeO_{12}$ phases", *J. Solid State Chem.*, **151** (2000) 323–325.
5. R.A. Zaman, M.J. Abu, J.J. Mohamed, M.F. Ain, Z.A. Ahmad, "Investigation of the mixing medium effect on the development of the CCTO microstructure at 1000 °C", *Procedia Chem.*, **19** (2016) 906–909.
6. P. Liu, Y. Lai, Y. Zeng, S. Wu, Z. Huang, J. Han, "Influence of sintering conditions on microstructure and electrical properties of $CaCu_3Ti_4O_{12}$ (CCTO) ceramics", *J. Alloys Compd.*, **650** (2015) 59–64.
7. S. Almeida-Didry, M.M. Nomel, C. Autret, C. Honstettre, A. Lucas, F. Pacreau, F. Gervais, "Control of grain boundary in alumina doped CCTO showing colossal permittivity by core shell approach", *J. Eur. Ceram. Soc.*, **38** (2018) 3182–3187.
8. S. Almeida-Didry, C. Autret, A. Lucas, C. Honstettre, F. Pacreau, F. Gervais, "Leading role of grain boundaries in colossal permittivity of doped and undoped CCTO", *J. Eur. Ceram. Soc.*, **34** (2014) 3649–3654.
9. J. Zhang, J. Zheng, Y. Li, Y. Liu, W. Hao, L. Lin, Y. Li, J. Song, "Effect of different pH values adjusted by ammonia on the dielectric properties of $CaCu_3Ti_4O_{12}$ ceramics prepared by a sol-gel method", *J. Alloys Compd.*, **779** (2019) 255–260.
10. L. Zhao, R. Xu, Y. Wei, X. Han, C. Zhai, Z. Zhang, X. Qi, B. Cui, J.L. Jones, "Giant dielectric phenomenon of $Ba_{0.5}Sr_{0.5}TiO_3/CaCu_3Ti_4O_{12}$ multilayers due to interfacial polarization for capacitor applications", *J. Eur. Ceram. Soc.*, **39** (2019) 1116–1121.
11. X. Huang, Y. Jiang, K. Wu, "CCTO giant dielectric ceramic prepared by reaction sintering", *Procedia Eng.*, **102** (2015) 468–474.
12. S. Kaur, A. Kumar, A.L. Sharma, D.P. Singh, "Dielectric and energy storage behavior of $CaCu_3Ti_4O_{12}$ nanoparticles for capacitor application", *Ceram. Int.*, **45** (2019) 7743–7747.
13. M. Ahmadipour, M.F. Ain, S. Goutham, Z.A. Ahmad, "Effects of deposition time on properties of $CaCu_3Ti_4O_{12}$ thin film deposited on ITO substrate by RF magnetron sputtering at ambient temperature", *Ceram. Int.*, **44** (2018) 18817–18820.
14. R. Schmidt, M.C. Stennett, N.C. Hyatt, J. Pokorny, J.P. Gonjal, M. Li, D.C. Sinclair, "Effects of sintering temperature on the internal barrier layer capacitor (IBLC) structure in $CaCu_3Ti_4O_{12}$ (CCTO) ceramics", *J. Eur. Ceram. Soc.*, **32** (2012) 3313–3323.
15. S. Guillemet-Fritsch, Z. Valdez-Nava, C. Tenailleau, T. Lebey, B. Durand, J.Y. Chane-Ching, "Colossal permittivity in ultrafine grain size $BaTiO_{3-x}$ and $Ba_{0.95}La_{0.05}TiO_{3-x}$ materials", *Adv. Mater.*, **20** (2008) 551–555.
16. Z. Song, S. Zhang, H. Liu, H. Hao, M. Cao, Q. Li, Q.

Wang, Z. Yao, Z. Wang, M.T. Lanagan, "Improved energy storage properties accompanied by enhanced interface polarization in annealed microwave sintered BST", *J. Am. Ceram. Soc.*, **98** (2015) 3212–3222.
17. D.M. Supriya, M.R. Rajani, A.R. Phani, C.V.S. Naveen, R. Ravishankar, "Synthesis of CCTO and doped CCTO nanopowders and its applications in the field of electronics", *Mater. Today-Proc.*, **4** (2017) 12021–12025.
18. R. Espinoza-González, S. Hevia, A. Adrian, "Effects of strontium/lanthanum co-doping on the dielectric properties of $CaCu_3Ti_4O_{12}$ prepared by reactive sintering", *Ceram. Int.*, **44** (2018) 15588–15595.
19. L. He, J.B. Neaton, M.H. Cohen, D. Vanderbilt, C.C. Homes, "First-principles study and lattice dielectric response of $CaCu_3Ti_4O_{12}$", *Phys. Rev. B*, **65** (2002) 214112.
20. D.C. Sinclair, T.B. Adams, F.D. Morrison, A.R. West, "$CaCu_3Ti_4O_{12}$ one-step internal barrier layer capacitor", *Appl. Phys. Lett.*, **80** (2002) 2153–2155.
21. M. Ahmadipour, W.K. Cheah, M.F. Ain, K.V. Rao, Z.A. Ahmad, "Effects of deposition temperatures and substrates on microstructure and optical properties of sputtered CCTO thin film", *Mater. Lett.*, **210** (2018) 4–7.
22. N. Akcay, N.A. Sonmez, E.P. Zaretskaya, S. Ozcelik, "Influence of deposition pressure and power on characteristics of RF-Sputtered Mo films and investigation of sodium diffusion in the films", *Curr. Appl. Phys.*, **18** (2018) 491–499.
23. C.R. Foschini, R. Tararam, A.Z. Simões, M. Cilense, L.S. Rocha, C.O.P. Santos, E. Longo, J.A. Varela, "Rietveld analysis of $CaCu_3Ti_4O_{12}$ thin films obtained by RF-sputtering", *J. Mater. Sci.: Mater. Electron.*, **27** (2016) 2175–2182.
24. R. Savu, J.A. Varela, M.S. Castro, P.R. Bueno, E. Joanni, "P-type semiconducting gas sensing behavior of nanoporous rf sputtered $CaCu_3Ti_4O_{12}$ thin films", *Appl. Phys. Lett.*, **92** (2008) 132110–132112.
25. M. Ahmadipour, S.N. Ayub, M.F. Ain, Z.A. Ahmad, "Structural, surface morphology and optical properties of sputter-coated $CaCu_3Ti_4O_{12}$ thin film: Influence of RF magnetron sputtering power", *Mater. Sci. Semicon. Proc.*, **66** (2017) 157–161.
26. L. Wu, Y. Zhu, S. Park, S. Shapiro, G. Shirane, J. Tafto, "Defect structure of the high-dielectric-constant perovskite $CaCu_3Ti_4O_{12}$", *Phys. Rev. B*, **71** [1] (2005) 014118–014125.
27. V. Brizé, G. Gruener, J. Wolfman, K. Fatyeyeva, M. Tabellout, M. Gervais, "Grain size effects on the dielectric constant of $CaCu_3Ti_4O_{12}$ ceramics", *Mater. Sci. Eng. B*, **129** [1-3] (2006) 135–138.
28. A.I. Kingon, J.P. Maria, S.K. Streiffer, "Alternative dielectrics to silicon dioxide for memory and logic devices", *Nature*, **406** (2000) 1032–1038.
29. J. Robertson, "High dielectric constant oxides", *Eur. Phys. J. Appl. Phys.*, **28** (2004) 265–291.
30. T. Wang, J.G. Ekerdt, "Structure versus thermal stability: The periodic structure of atomic layer deposition-grown Al-incorporated HfO_2 films and its effects on amorphous stabilization", *Chem. Mater.*, **23** (2011) 1679–1685.
31. K. Yang, X. Huang, Y. Huang, L. Xie, P. Jiang, "Fluoropolymer-$BaTiO_3$ hybrid nanoparticles prepared via RAFT polymerization: Toward ferroelectric polymer nanocomposites with high gielectric constant and low gielectric loss for energy storage application", *Chem. Mater.*, **25** (2013) 2327–2338.
32. R.Z. Hou, A. Wu, P.M. Vilarinho, "Low-temperature hydrothermal deposition of $(Ba_xSr_{1-x})TiO_3$ thin films on flexible polymeric substrates for embedded applications", *Chem. Mater.*, **21** (2009) 1214–1220.
33. B. He, Z. Wang, "Enhancement of the electrical properties in $BaTiO_3/PbZr_{0.52}Ti_{0.48}O_3$ ferroelectric superlattices", *ACS Appl. Mater. Interfaces*, **8** (2016) 6736–6742.
34. E. Brown, C. Ma, J. Acharya, B. Ma, J. Wu, J. Li, "Controlling dielectric and relaxor-ferroelectric properties for energy storage by tuning $Pb_{0.92}La_{0.08}Zr_{0.52}Ti_{0.48}O_3$ film thickness", *ACS Appl. Mater. Interfaces*, **6** (2014) 22417–22422.
35. R.A. Young, A. Sakthivel, T.S. Moss, C.O. Paiva-Santos, "*DBWS*-9411 - an upgrade of the *DBWS**.* programs for Rietveld refinement with PC and mainframe computers", *J. Appl. Cryst.*, **28** (1995) 366–367.
36. P. Jha, P. Arora, A.K. Ganguli, "Polymeric citrate precursor route to the synthesis of the high dielectric constant oxide $CaCu_3Ti_4O_{12}$", *Mater. Lett.*, **57** (2003) 2443–2446.
37. A.A. Felix, E. Longo, J.A. Varela, M.O. Orlandi, "Gas sensing and conductivity relationship on nanoporous thin films: A $CaCu_3Ti_4O_{12}$ case study", *Thin Solid Films*, **604** (2016) 69–73.
38. T. Li, R. Xue, J. Hao, Y. Xue, Z. Chen, "The effect of calcining temperatures on the phase purity and electric properties of $CaCu_3Ti_4O_{12}$ ceramics", *J. Alloy. Compd.*, **509** [3] (2011) 1025–1028.
39. A.F.L. Almeida, R.E.S. Oliveira, J.M. Sasaki, A.S.B. Sombra, L.C. Kretly, "Electrical and optical properties of $CaCu_3Ti_4O_{12}$ (CCTO) substrates for microwave devices and antennas", *Micro. Opt. Technol. Lett.*, **39** (2003) 145–150.
40. J.F. Moulder, W.F. Stickle, P.E. Sobol, K.D. Bomben, *Handbook of X-ray Photoelectron Spectroscopy*, Perkin-Elmer Corporation, Physical Electronis Division, Eden Prairie, Minessota, 1992.
41. P.R. Bueno, R. Tararam, P. Parra, E. Joanni, J.A. Varela, "A polaronic stacking fault defect model for $CaCu_3Ti_4O_{12}$ material: an approach for the origin of the huge dielectric constant and semiconducting coexistent features", *J. Phys. D Appl. Phys.*, **42** (2009) 1–9.